Engineering plasmonic charge kinetics and broadband photoelectrochemical spectral response using multi-resonant Au-TiO_2 plasmonic particle grating based optical resonator

[1]Saurabh Pandey, [1]Shereena Joseph, [2]Shubhangi Majumdar, [1]Jagriti Ahuja, [3]Shital Devinder, [4]Shumile Ahmed Siddiqui, [4]Kaushik Ghosh, and [1,5]Joby Joseph[#]

[1]Photonics Research Lab, Physics Department, Indian Institute of Technology, Delhi, New Delhi, Delhi, 110016, India

[2]Physical & Bio-physical Chemistry Research Lab, Department of Chemistry, Indian Institute of Technology, Delhi, New Delhi, Delhi, 110016, India

[3]Centre for Sensors, Instrumentation, and Cyber Physical System Engineering, Indian Institute of Technology Delhi, New Delhi, Delhi, 110016, India

[4]Institute of Nano Science & Technology, Knowledge City, Sector-81, SAS Nagar, Manauli PO 140306, Punjab, India

[5]Optics and Photonics Centre, Indian Institute of Technology Delhi, New Delhi, Delhi, 110016, India

E-mail: joby@iitd.ac.in

Supporting Information:

S1: Structural and optical characterization

The band gap of titanium dioxide (TiO_2) thin film deposited over ITO-coated glass was calculated using the Tauc plot method. The absorption spectra were calculated using the home-built UV-Vis spectrometer. Absorption spectra of bare ITO-coated glass were taken as the reference to calculate the absorption spectra of the thin TiO_2 film alone. The Tauc equation for semiconductor material is given by

$$(\alpha \cdot h\upsilon)^{1/n} = B(h\upsilon - Eg) \quad (1)$$

where h is the Plank constant, υ is photon frequency, E_g is band gap energy, B is a constant, n is a factor that depends on electron transition property, and α is the absorbance coefficient. The value of n is ½ and 2 for direct and indirect band gap transition, respectively. The absorbance coefficient

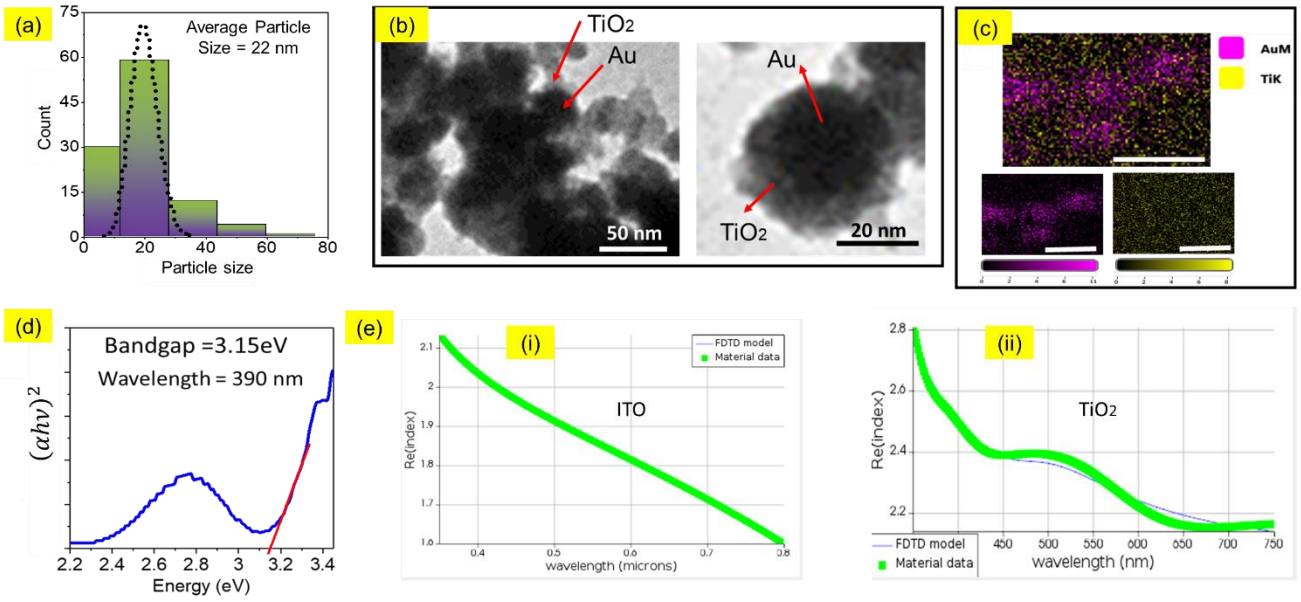

Figure S1 (a) Gold nanoparticle size distribution of PPG photoelectrode, (b) HRTEM images of PPG-TIO_2, (c) FESEM-EDX characterized elemental mapping for Au and Ti of TiO_2, (d) Tauc plot of TiO_2 film deposited over ITO coated glass for band gap calculation of TiO_2, ellipsometry spectroscopy characterization of (e) (i) ITO coated over glass for getting refractive index, (ii) TiO_2 coated over PPG.

is calculated by $\frac{1}{t}\log_{10}(T(\%))$, where T is the recorded transmittance and 't' is the thickness of the TiO_2 medium.

In the Figure S1(b), Au and TiO_2 layer can be distinguished. It is evident that Au is not everywhere is surrounded by 40 nm thick TiO_2 layer. Depending on how these nanoparticles are closely packed, surrounding TiO_2 layer from sides can vary. For elemental mapping, we are providing here FESEM-EDAX characterized elemental mapping with best of the resolution possible with FESEM –TESCAN model: Magna LMU. We omitted the element coming from the substrate SiO_2 and ITO including oxygen to get a better elemental mapping of interested elements, as provided in the Figure S1(c).

The band gap energy is calculated using the Tauc plot, as shown in Figure S1(d), where the intersection with the energy axis represents an estimate of the relevant energy gap. Based on this calculation, we determined that the band gap energy of TiO_2 material is 3.15 eV.

S2: Optical modes investigation with dielectric grating

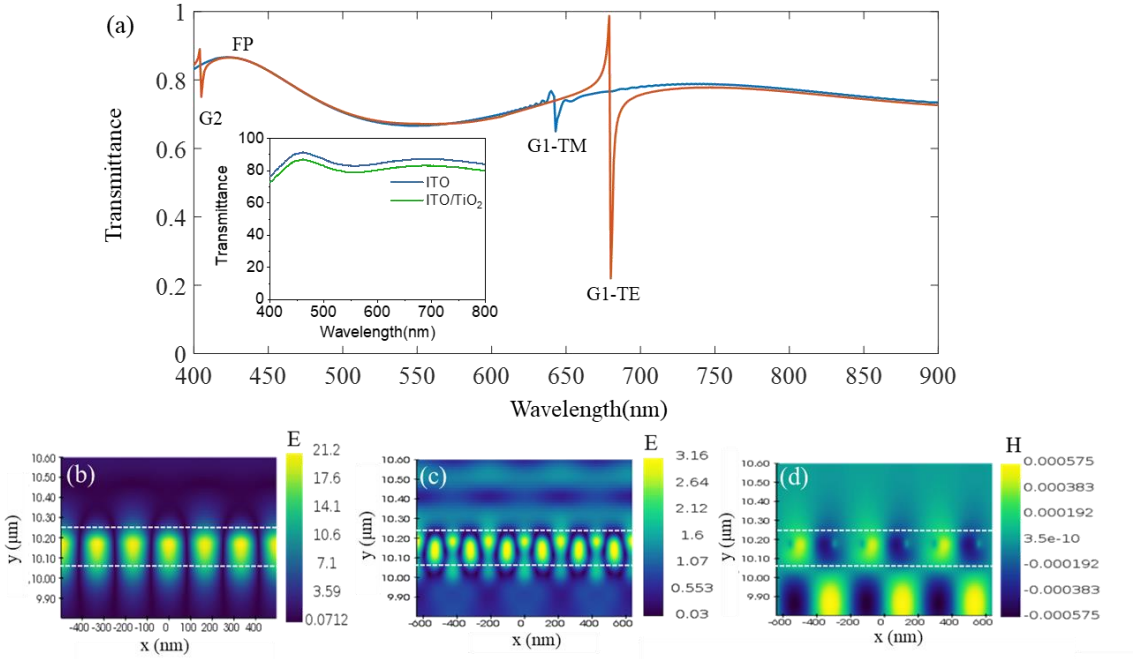

Figure S2: Optical transmittance of dielectric grating (Si_3N_4) over ITO waveguide covered with TiO_2(40nm), (a) FDTD simulated optical transmittance for TM and TE incidence. Inset shows the experimentally obtained transmittance for ITO and TiO_2 coated on ITO, revealing existence of Fabry Perot mode ≈ 450 nm. E field and H field profile of G1, G2 and FP mode (b), (c), (d) respectively

The most straightforward approach to distinguish the plasmon occurring with photonic mode is considering the grating of the dielectric medium. Through FDTD simulation, we replaced the metal grating with Si_3N_4 dielectric grating, revealing only photonic mode, i.e., guided-mode resonance for 1st and 2nd order along with weak FP mode, as shown in Figure S2(a). These photonic modes are validated through electric field distribution, as shown in Figure S2(b-d).

S3. Plasmonic response in random gold nanoparticles

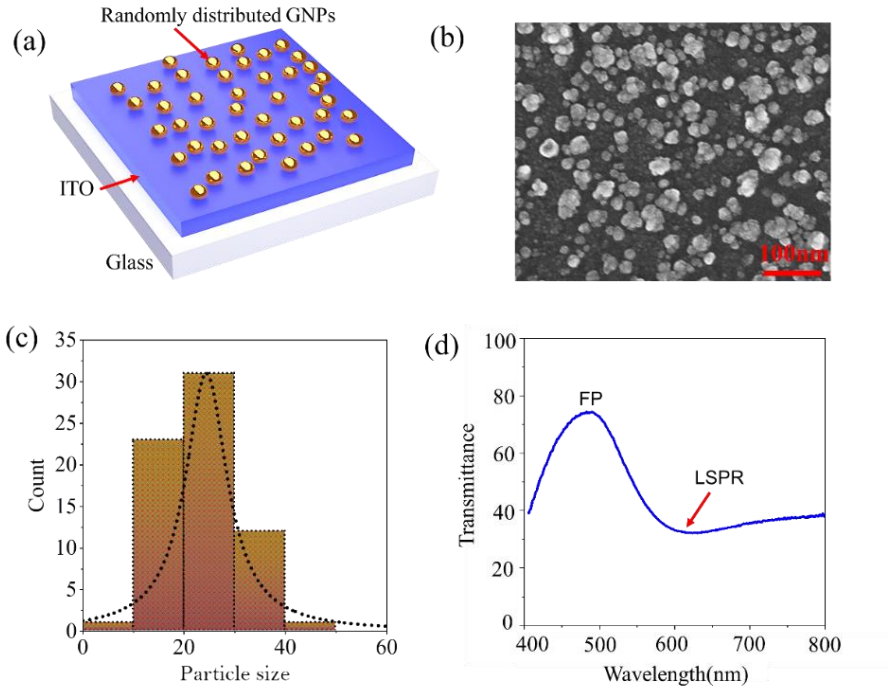

Figure S3: (a) An schematic illustration of random gold nanoparticles distribution over ITO waveguide over glass substrate, (b) FESEM image, (c) particle size distribution and (d) optical transmittance spectra, revealing LSPR excitation ≈ 520nm – 750nm.

We have deposited random gold nanoparticles with electrochemical deposition over an ITO waveguide of comparable size, as shown in Figure S3(a-c), displaying a broadband dip in transmittance as shown in Figure S3(d), corresponding to plasmonic resonance along with FP

mode formed in the ITO waveguide. We noticed red shift of FP peak wavelength than dielectric grating or ITO film due to extra phase imparted by the metallic nanoparticles. We observed the same transmittance drop after FP mode with broadband transmittance with PPG-TiO_2 under TM and TE incidence, as shown in Figure S3(d) and Figure 4(a).

S4. The PPG-TiO_2 and PSG-TiO_2 optical transmittance

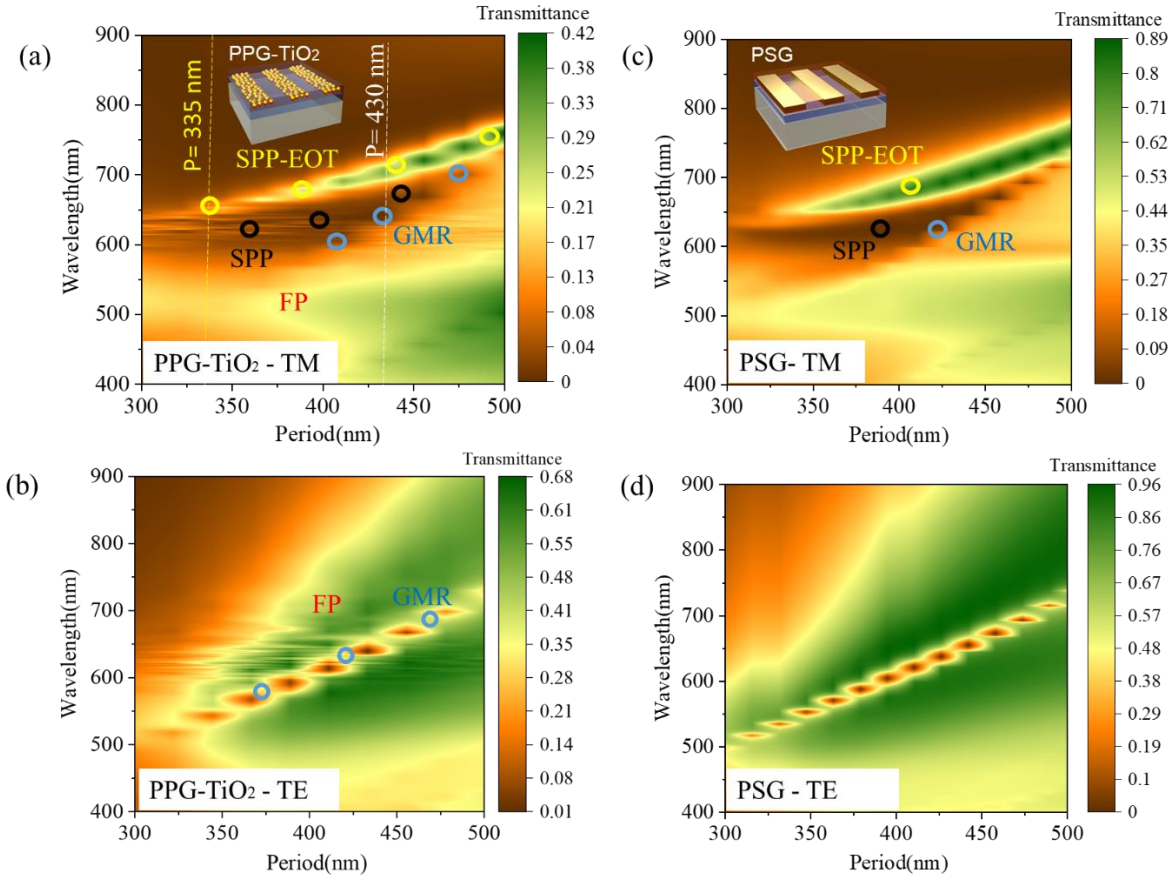

Figure S4. Optical transmittance contour plot with varying width of grating under for (a) TM incidence, (b) TE incidence for PPG-TiO_2 structural configuration, and similarly for PSG in (c,d).

Figure S4 shows the optical mode behavior with the period of the gratings in plasmonic particle and plasmonic slab grating. In TE incidence, the GMR1 mode is excited in the vicinity of a broad Fabry-Perot kind of background resonance incidence, resulting in a broad asymmetric peak due to FP-GMR interaction, which is evident for period sweep (Figure S4(b,d)).

S5: Fabry Perot and collective LSPR interaction under TE and TM incidence

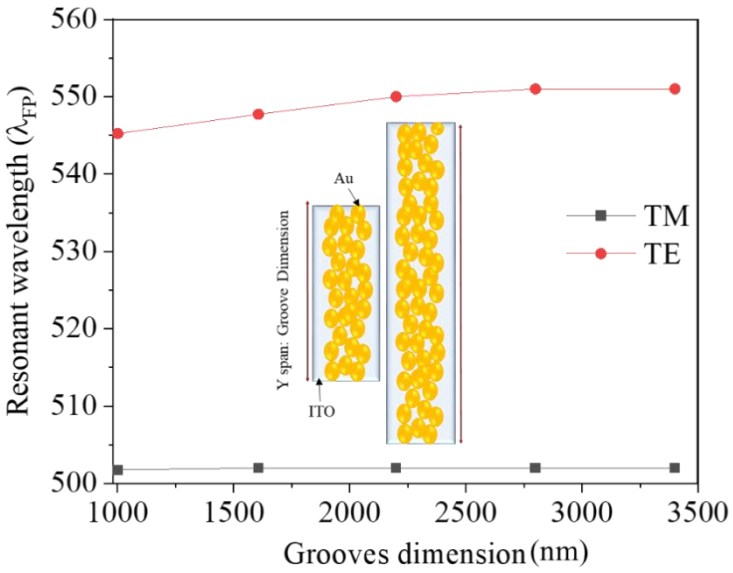

Figure S5: Variation of the FP-collective LSPR resonant wavelength while increasing the groove dimension along Y axis for TM and TE incidence. An illustration of number of particles increases with the Y span of the grating is shown in the inset of the graph.

The variation of FP-collective LSPR resonant wavelength was studied with FDTD solver by varying the Y span of the FDTD region, corresponding to more numbers of gold nanoparticles along the Y axis. As we increase the Y span, the number of plasmonic dipoles increases. As, a result, the large number of dipole axis aligned in the direction of electric field direction in TE incidence. While the number of particles along the X span remains fixed. We observed no appreciable change for TM incidence, while redshift was observed for TE incidence, which gets saturated for at higher groove length.

S6. The electric field distribution of grating coupled plasmon mode with plasmonic slab grating

The mode evolution of grating coupled surface plasmon polariton mode (SPP) was investigated numerically, considering the metallic slab grating to avoid the complex electric field distribution and reduce the simulation time compared to PPG. Figure S6(a) shows the $n_{effective}$ calculation for SPP excitation and diffracted order, defined by equations 1 and 2[1], respectively, defined as

$$\text{neff} = \sqrt{\frac{\text{Re}(\varepsilon_{Au})\varepsilon_{ITO}}{\text{Re}(\varepsilon_{Au})+\varepsilon_{ITO}}} \quad (1)$$

$$\text{neff} = \frac{m\lambda}{p} \tag{2}$$

where, $\text{Re}(\varepsilon_{Au})$ and ε_{ITO} are real and absolute dielectric permittivity of the Au and ITO, which depends on the wavelength, p is the grating period, and m is the diffracted order. Figure S6(a) confirms the SPP excitation (≈660nm) at the ITO-Au interface with 1st-order diffracted order. In the simulation studies, we noticed no spectral variation in SPP mode with and without a TiO_2 layer over the Au grating structure, which indicates that SPP originated only from the Au-ITO interface.

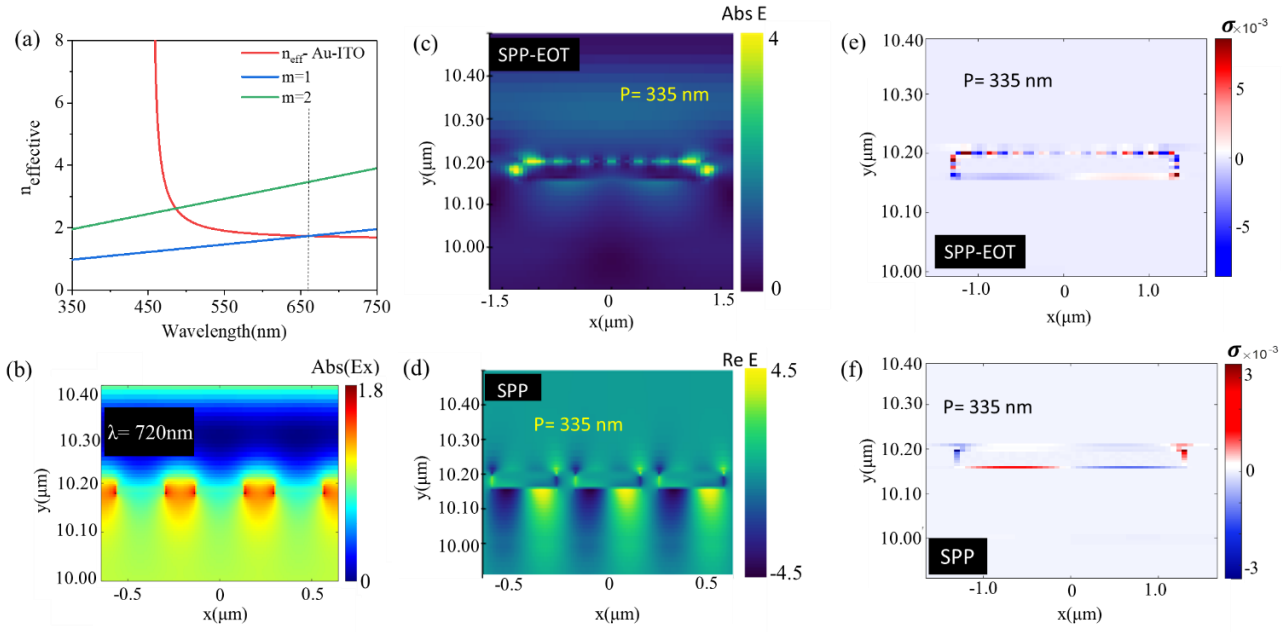

Figure S6. (a) SPP dispersion relation plot with diffracted order m=1, m=2 for ITO-Au interface, (b) Electric field distribution corresponding to cavity mode at wavelength 720nm, Electric field distribution (c)SPP-EOT, (d) SPP plasmon mode with respective charge distribution (e) and (f) respectively.

Figure S6(b) demonstrates the electric field distribution at wavelength 720, illustrating the cavity mode formation with the metallic slits due to in-plane diffraction near Rayleigh wavelength, which results in SPP-EOT mode formation through evanescent electromagnetic field coupling of SPP and cavity mode. Figure S6(c,d) shows the electric field distribution for SPP-EOT, SPP mode at period 335 nm, where these modes are spectrally separated, with their charge distribution is displayed in Figure S6(e.f).

S7. Optimization of TiO_2 thickness:

The thickness of TiO_2 plays a vital role in plasmonic charge collection and its accessibility for PEC activities. Ideally, it should be thinner to better charge diffusion, avoiding charge recombination and further relaxation in TiO_2 to be accessible for PEC reactions at its surface. However, due to its dielectric characteristics, the TiO_2 layer is a diffusion layer and can assist in the optical coupling of incident light with Au nanoparticles. Therefore, the optimal thickness of TiO_2 for optimal local electromagnetic field density localization needs to be found, which ultimately governs the production of plasmonic charge carriers, i.e., $\propto |E|^2$ [2,3]. Figure S7(a) demonstrates the optical mode evolution with a thickness of TiO_2 layer, which conveyed the strong interaction of the SPP and SPP-EOT for TiO_2 thickness ≈ 40 nm, while no such interactions are noticed in TE incidence due to passive SPP mode (Figure S7(b)). Based on prime local hotspots, the PEC performance can also be enhanced for larger thicknesses, as reported in literature[4–6], which focuses on optical mode-enhanced photocurrent generation.

Secondly, the TiO_2 film of the TiO_2-Au nano-hybrid layer provides an electron receptor and a diffusion layer for transporting the hot electrons from the back electrode to the Pt counter electrode. Here, it should be noted that low Schottky interface area to receive electrons while increasing the thickness benefits the electron reception. The combined effect of both functions will decide the

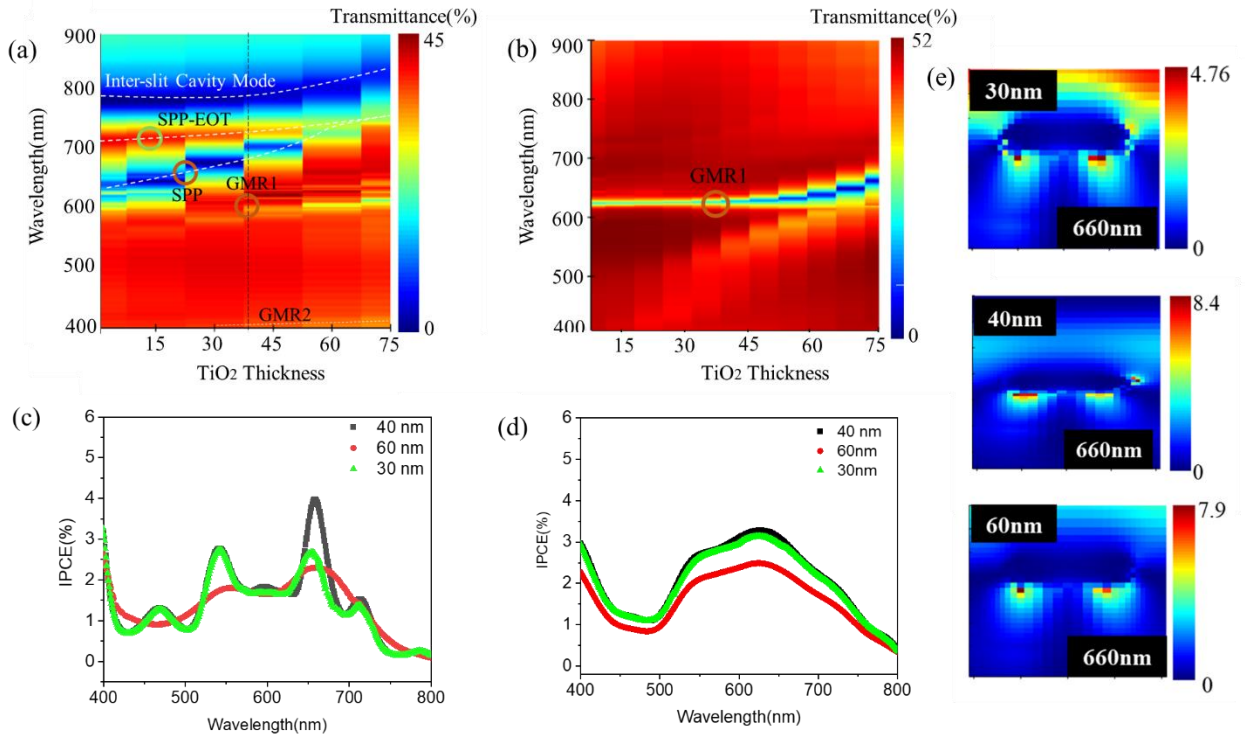

Figure S7. Transmittance spectra with varying thickness of TiO_2 layer for (a) TM incidence, revealing SPP-EOT and SPP mode interaction for thickness 40 nm of TiO_2, (b) TE incidence with no active SPP mode. (c,d) IPCE plot TiO_2 thickness 40, 60, and 30 nm under TM and TE incidence respectively, (e)) $|E|^2$ plot for SPP-EOT interaction at thickness 30nm, 40 nm 60 nm respectively.

optimized photocurrent. The average size of the gold nanoparticles in the porous gold nanoparticle grooves is about 22 nm. To get large Schottky interface area to receive electrons, the nanoparticles should be perfectly covered from the sides and upper surface, i.e., the thickness of TiO_2 is required to be deposited >22 nm. Here, it should also be noted that the grating is porous and consists of closely packed gold nanoparticles, which leads to the lower thickness of the TiO_2 layer surrounding the gold nanoparticles from the sides and aids in charge diffusion. Therefore, the actual thickness of TiO_2 layer covered from the sides of the plasmonic particles will be sufficient less defined by the inter-particle spacing, and aids for hole diffusion towards surface of the Au-TiO_2 hybrid electrode.

The utilization of optical and electrical properties can be efficiently achieved with a 40 nm TiO_2 layer. To illustrate this, the photoelectrochemical (PEC) spectrum response was tested for TiO_2 thicknesses (30 nm, 40 nm and 60 nm), as shown in the Figure S7(c, d) for TM and TE incidence case. IPCE versus wavelength curve in Figure S7(d) for TE illumination, define no appreciable IPCE changes with TiO_2 thickness 40 and 30 nm, while relatively a significant drop can be observed for 60 nm accompanied by the relatively poor diffusion of charges. Whereas, a significant change in IPCE was observed for TM incidence in all three samples in the spectral domain of plasmonic and diffractive coupled plasmon resonance. Figure S7(e) demonstrates the electric field distribution at wavelength 660 nm corresponding to the strong interaction of the SPP and SPP-EOT, which shows in spite of having comparable electric field localization IPCE spectra corresponding to 60 nm shifted down compared to 40 nm thickness of the TiO_2 layer, which is again due to poor diffusion of charges in the TiO_2 medium. However, for the thickness 30 nm, a significant drop corresponding to SPP-EOT peak and GMR peak with blue shift was observed, due to weak interaction of GMR, SPP and SPP-EOT, as shown in Figure S7(a), resulting in low confinement of electromagnetic field (Figure S7(e)).

S8. Experimental setup of IPCE measurement:

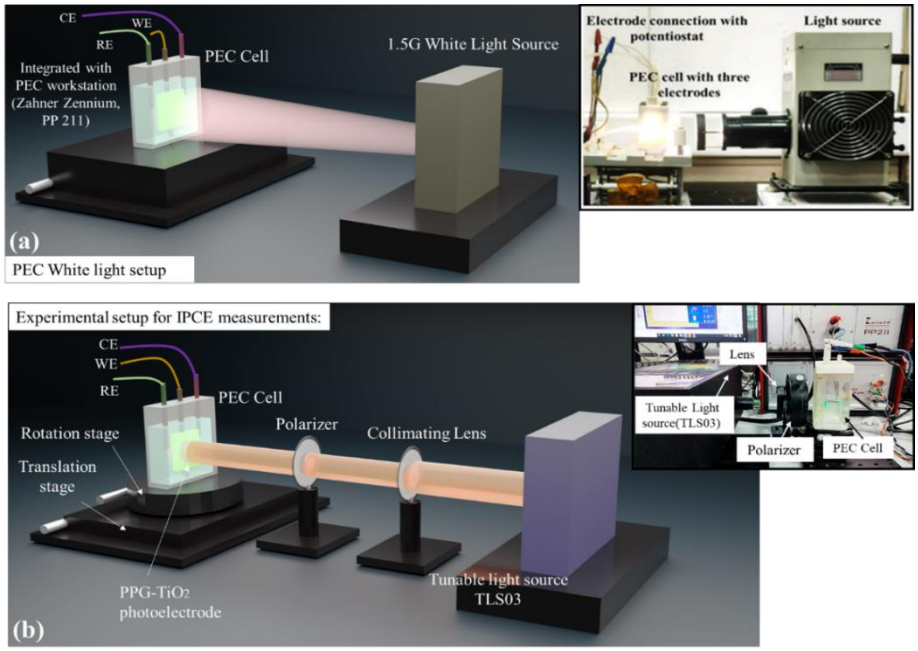

Figure S8. Experimental setup for (a) White light photo-electrochemical(PEC) measurements, (b) Polarization dependence Incident photon to electron conversion efficiency (IPCE) measurements.

S9: Stability of the Au-TiO_2 plasmonic particle grating photoelectrode

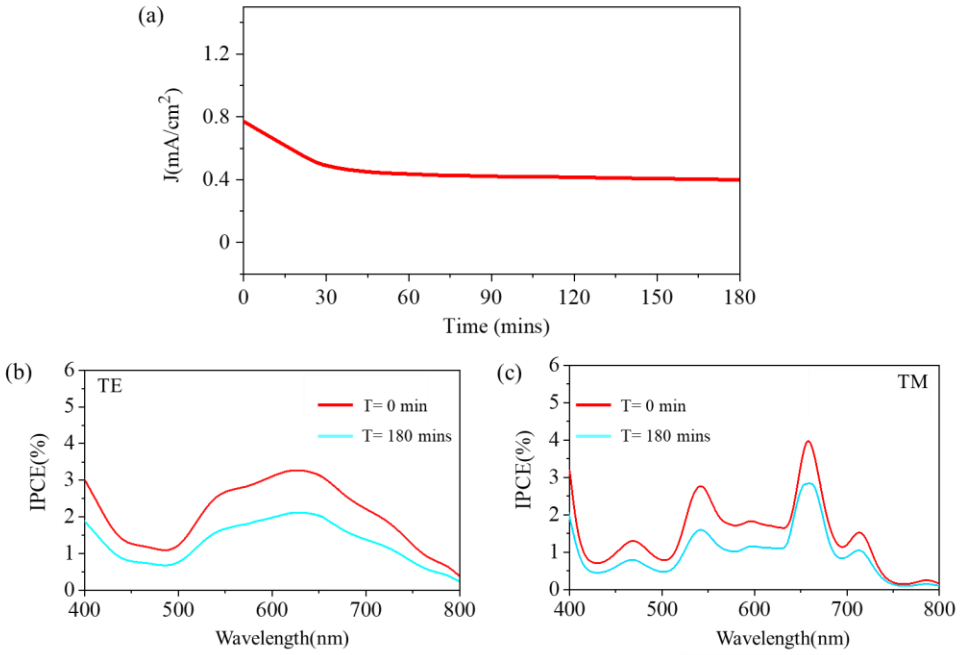

Figure S9. (a) Stability test of PPG-TiO_2 photoelectrode at 1V vs Ag/AgCl for 3 hrs (180 minutes), IPCE spectra at t = 0 and t = 180mins for (b) TM (c) TE incidence.

Figure S9 (a) shows the stability test for the photoelectrode for 3 hours' durations. However, we cannot extend this time due to the source's inability to operate under continuous working conditions for an extended period. In addition, Figure S9 (b), (c) shows IPCE measurements for TE and TM incidence, respectively, after 3 hours (180 minutes) of continuous PEC operation to support the long-term stability of the photoelectrode, with a similar trend, as exhibited by the IPCE measured at t = 0 minutes. A slight reduction in current density was evident in PEC and IPCE measurements. However, the constant current density profile (t>40 minutes) establishes it as suitable for the long run. IPCE measurement at t=0 and t = 180 minutes validated the long-term stability of SPP-GMR effect-induced photo-activity.

S10. Optical mode enhanced PEC current:

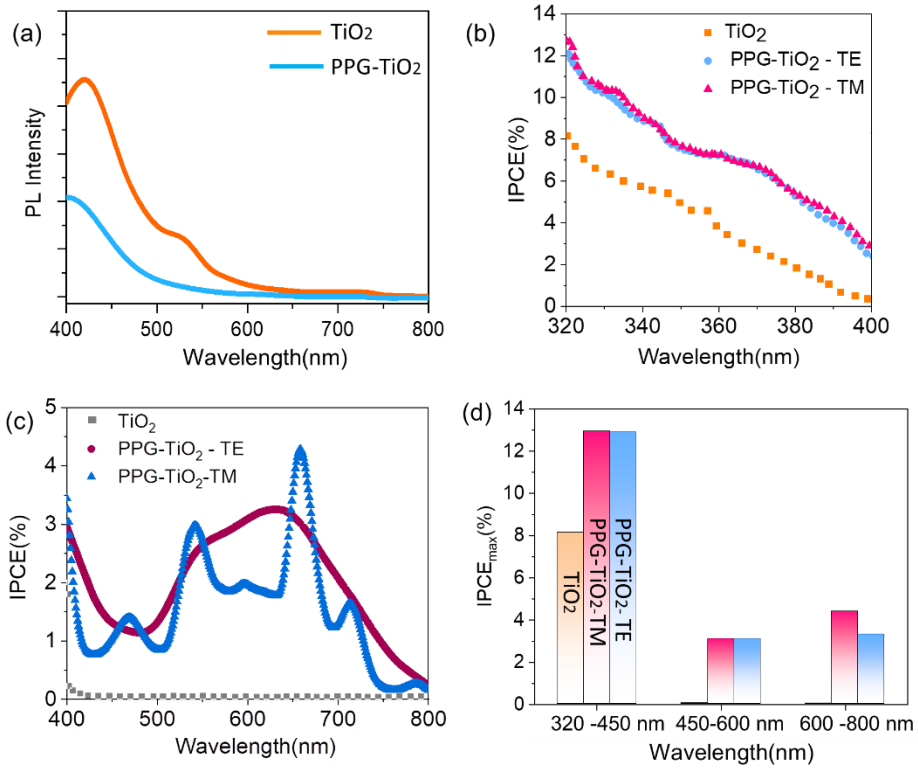

Figure S10. (a) Steady state photoluminescence emission spectra of PPG-TiO_2 and bare TiO_2 film, (b) IPCE (%) spectral response in UV region (320 nm-400 nm) for PPG-TiO_2 for TM and TE illumination, and TiO_2 film, (c) IPCE (%) spectral response in visible region (400 nm-800 nm) for PPG-TiO_2 for TM and TE illumination, and TiO_2 film., (d) maximum IPCE (%) obtained for different spectral region for photoelectrodes TiO_2, PPG-TiO_2 for TM and TE incidence.

Figure S10 illustrates the optical mode-enhanced PEC photoelectrochemical current generation. Figure S10 (a) represents the steady-state PL spectra for TiO_2 and Au-TiO_2 photoelectrodes. The

PL quenching confirms the relatively low charge recombination and enhanced charge availability for PEC chemical reactions. The observed PEC photocurrent improvement was further confirmed by steady-state photoluminescence spectra (Figure S10(a)), revealing PL quenching in Au-TiO2 than pure TiO2 photoelectrode. The PL quenching of TiO_2 in presence of Au nanoparticles can be mediated by non-radiative tunneling transitions mechanism[7], and through the absorption of the PL radiative energy by the gold nanoparticles due to the spectral overlapping of PL emission of TiO2 with the plasmonic resonance[8,9]. In both cases, the charge available for PEC current generation increases.

Figure S10(c) illustrates a direct comparison of PPG-TiO_2 and TiO_2 PEC spectral responses in TM and TE incidence in visible and NIR regions, which validates the optical modes enhanced PEC activity. Figure S10(d) demonstrates the maximum IPCE obtained in UV, Vis, and NIR regions.

S11. Optical Modes at Oblique Incidence: GMR-SPP coupling

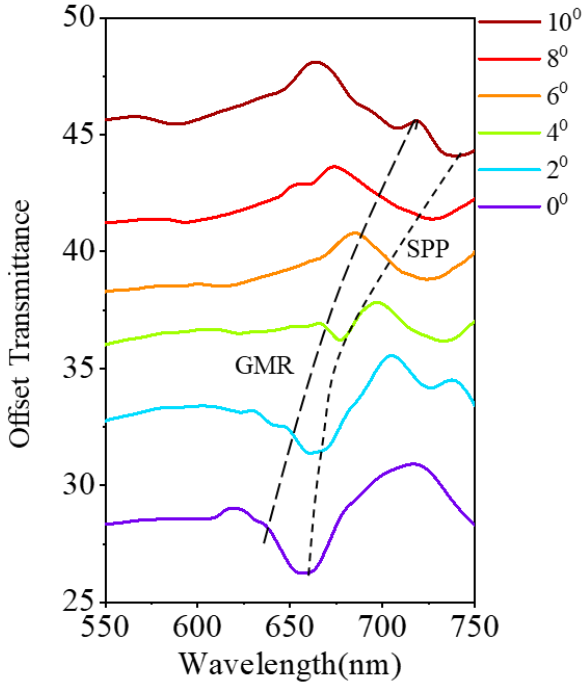

Figure S11. An offset transmittance plot for different angles of incidence shows the coupling of GMR-SPP.

Table ST1. Comparison of IPCE (%) for solar water splitting with Au-TiO_2 photoelectrode

Year	Working Electrode	Electrolyte/ pH	Mechanism	IPCE(%), J_{max}(Applied Potential)	Ref.
2016	Au–TiO_2 Nano sphere	Na_2SO_4 (0.5 M)/ pH = 2.6 adjusted with H_2SO_4	Wisper Gallery Mode enhanced plasmonic interaction	≤ 1.5%(-) ,120μA/cm^2 (-)	[6]
2017	TiO_2 nanotunnels (TNTs) loaded with gold nanoparticles (Au-NPs)	$KClO_4$	Plasmon induced charge separation, and plasmonic light absorption/scattering	≤ 0.8%(0.499 V vs. SHE) <1.0 mA/cm^2 (0.8V vs. SHE)	[10]
2018	Au-NP/TiO_2/Au-film	-	Strong mode coupling of Fabry–Pérot nanocavity modes with LSPR	≤ 1.5% (0.3 V vs SCE) -(-)	[11]
2019	Three-dimensional (3D) moth-eye AuNP/TiO_2/Au	0.5M Na_2SO_4/7.2	light trapping by moth-eye structure and enhanced surface plasmon resonance by gap-plasmon structure	≤ 3.5% (400nm-450nm) ≤ 0.02% (500nm-800nm) ≤ 100μA/cm^2 (1.6V vs. RHE)	[12]
2021	Au-Ag alloy nanoparticles/ TiO_2 thin film/Au film	KOH	LSPR- Fabry Perot Mode coupling	≤ 4% (0.5 V vs. Ag/AgCl) -(-)	[5]
2022	Pt/TiO_2/ Au nano-hole arrays nanocomposite	0.5M Na_2SO_4	SPP and LSPR	≤ 0.6% (0.5 V versus RHE) 30μA/cm^2 (0.9 vs. RHE) < 150μA/cm^2 (0.3 vs. RHE)	[13]
	TiO_2/Au-NPs one dimensional grating/ITO	1M KOH	Multi-resonant optical system (Fabry Perot, SPP,SPP-EOT,GMR)	≈ 4.4% (1V vs Ag/AgCl) ≈ 800 μA/cm^2 (1V vs. Ag/AgCl)	This work

S12: Ultrafast transient response of TiO_2

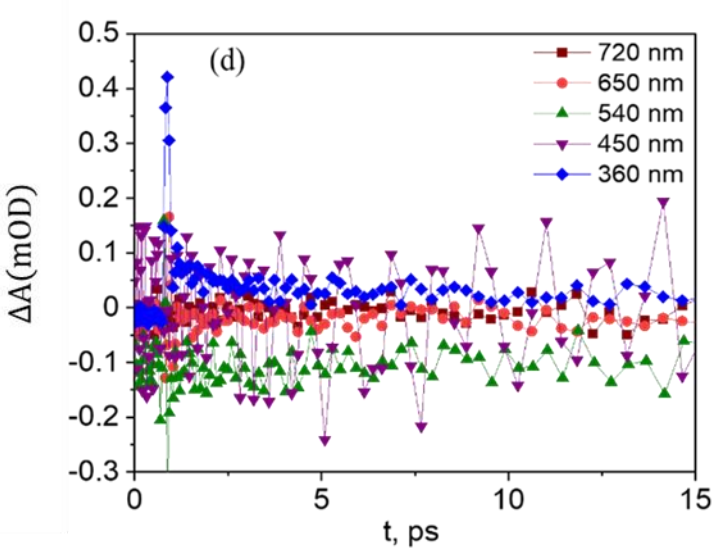

Figure S12: Transient absorption temporal response of TiO_2 bare film over ITO coated glass for different pump excitation at probe wavelength 500 nm.

S13. Decay time measurement through exponential decay fitting

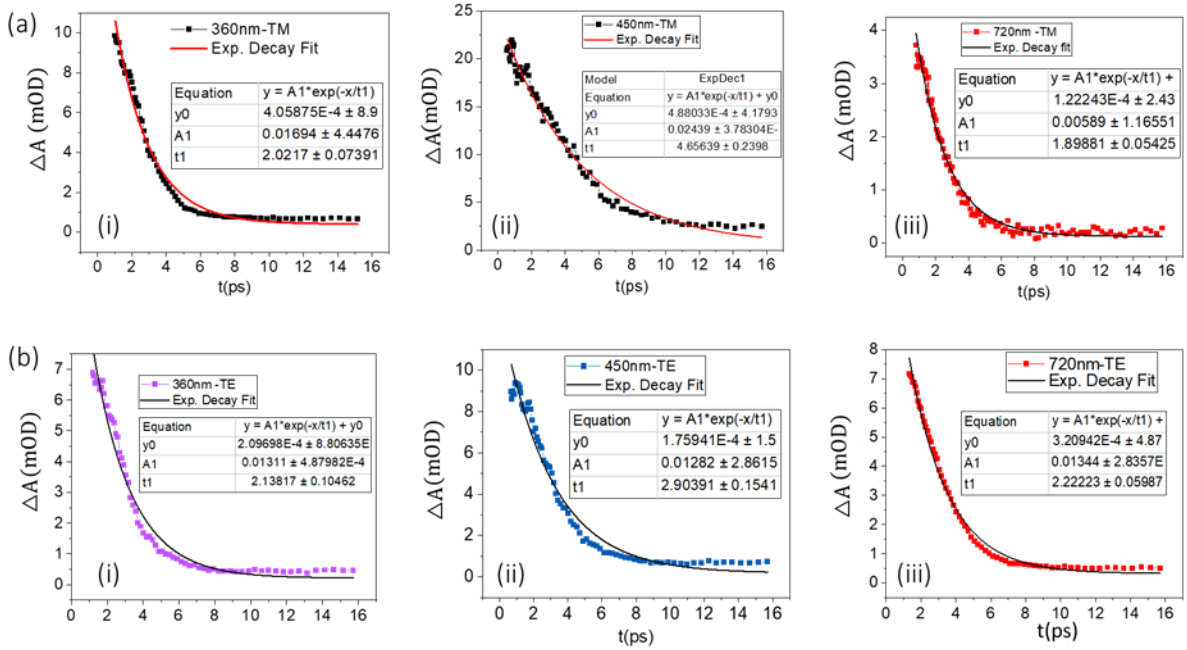

Figure S13: Exponential fitting of TA recorded 360nm,450nm and 720nm pump excitation at 500nm probe wavelength for (a)TM incidence, (b)TE incidence.

S14: Photonic modes impact on ultrafast transient absorption

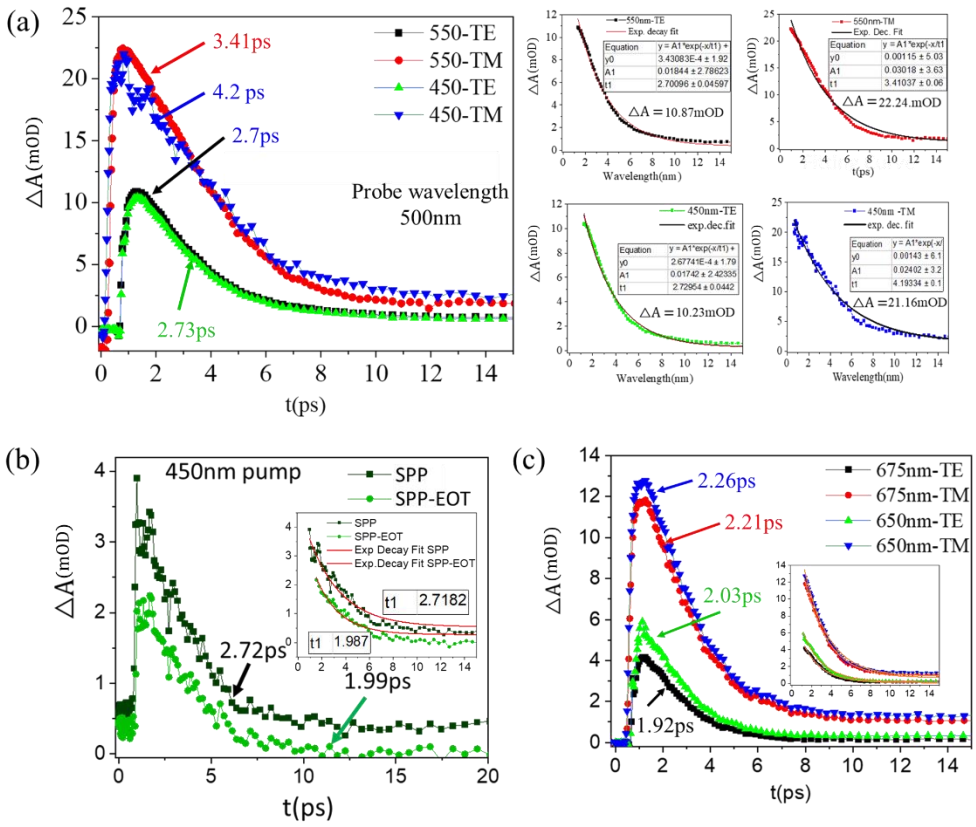

Figure S14. Pump probe investigation corresponding to different resonant states, (a) TA measurements at 500 nm probe wavelength with 450 nm, and 550 nm pump excitation under TM and TE incidence, with corresponding exponential decay fitting to evaluate the life time, (b) TA at probe wavelength 693 nm and 723 nm corresponding to SPP and SPP-EOT plasmonic mode under 450 nm pump excitation in TM illumination, (c) TA obtained in normal illumination with pump excitation wavelength 650 nm and 675nm with probe 500 nm under TM and TE incidence.

S15. Ultrafast Transient absorption near GMR-SPP coupled mode interaction

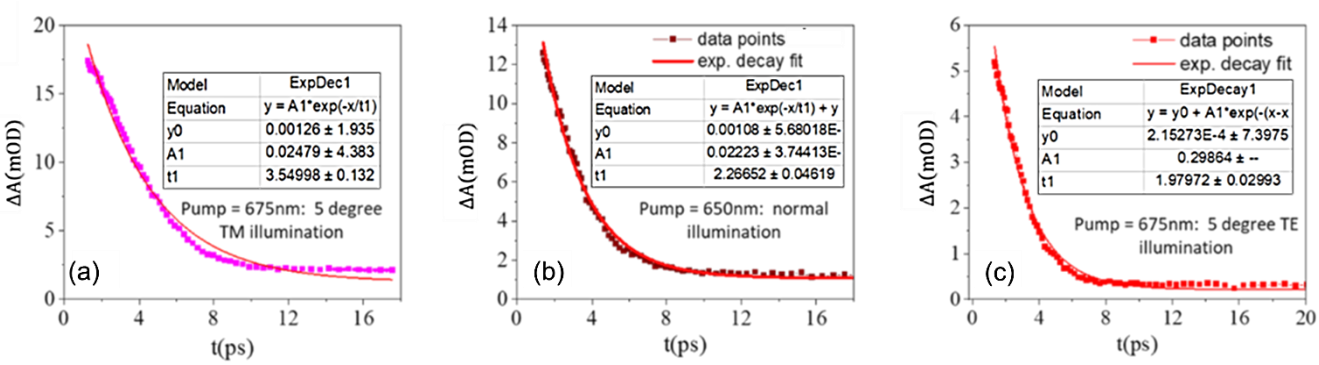

Figure S15. Pump probe investigation corresponding to coupled GMR- SPP mode, (a) pump =675 nm, probe =500 nm at 5^0, (b) pump =650 nm probe = 500nm at normal incidence in TM/TM illumination, (c) pump =675 nm, probe = 500 nm at 5^0 incidences, TE/TE illumination.

Table ST2: Transient change in absorption with calculated charge injection efficiency for PPG-TiO_2 under TM and TE incidence and for TiO_2.

Pump wavelength	PPG-TiO_2-TM (△Amax)	PPG-TiO_2-TM (△Amax)	TiO_2 (△Amax)	η-TM	η-TE
450nm	1.69mOD	1.10mOD	0.995mOD	1.1	1.24
550nm	2.87mOD	2.12mOD	0.363mOD	1.2	1.16
650nm	2.13mOD	1.98mOD	0.15mOD	1.41	1.3
720nm	1.46mOD	1.39mOD	0.1mOD	1.12	0.98

References:

1 S. Joseph, S. Sarkar and J. Joseph, *ACS Appl. Mater. Interfaces*, 2020, **12**, 46519–46529.

2 L. V. Besteiro, X. T. Kong, Z. Wang, G. Hartland and A. O. Govorov, *ACS Photonics*, 2017, **4**, 2759–2781.

3 M. L. Brongersma, N. J. Halas and P. Nordlander, *Nat. Nanotechnol.*, 2015, **10**, 25–34.

4 X. Shi, K. Ueno, T. Oshikiri, Q. Sun, K. Sasaki and H. Misawa, *Nat. Nanotechnol.*, 2018, **13**, 953–958.

5 Y. Suganami, T. Oshikiri, X. Shi and H. Misawa, *Angew. Chemie - Int. Ed.*, 2021, **60**, 18438–18442.

6 J. Zhang, X. Jin, P. I. Morales-Guzman, X. Yu, H. Liu, H. Zhang, L. Razzari and J. P. Claverie, *ACS Nano*, 2016, **10**, 4496–4503.

7 B. Guo, L. Tian, W. Xie, A. Batool, G. Xie, Q. Xiang, S. U. Jan, R. Boddula and J. R. Gong, *Nano Lett.*, 2018, **18**, 5954–5960.

8 and A. L. B. Xia Zhang, Cristian A. Marocico, Manuela Lunz, Valerie A. Gerard, Yurii K. Gun'ko, Vladimir Lesnyak, Nikolai Gaponik, Andrei S. Susha, Andrey L. Rogach, *ACS Nano*, 2012, **6**, 9283–9290.

9 and P. R. Pierre Viste, Jérome Plain, Rodolphe Jaffiol, Alexandre Vial, Pierre Michel Adam, *ACS Nano*, 2010, **4**, 759–764.

10 R. Takakura, T. Oshikiri, K. Ueno, X. Shi, T. Kondo, H. Masuda and H. Misawa, *Green Chem.*, 2017, **19**, 2398–2405.

11 X. Shi, K. Ueno, T. Oshikiri, Q. Sun, K. Sasaki and H. Misawa, *Nat. Nanotechnol.*, 2018, **13**, 953–958.

12 J. Jun, H. Kim, H. J. Choi, T. W. Lee, S. Ju, J. M. Baik and H. Lee, *Sol. Energy Mater. Sol. Cells*, 2019, **201**, 110033.

13 H. Jia, Z. Li, B. Wang, G.Xing, Y. L. Wong, H. Ren. M. Li, K. Y. Wong, D. Lei, L. W. Wong, J. Zhao, W. Zhang, S. Sang, A. Jian, X. Zhang, ACS Photonics 2022, 9, 2, 652–663